Bevacizumab-Induced Transient Remodeling of the Vasculature in Neuroblastoma Xenografts Results in Improved Delivery and Efficacy of Systemically Administered Chemotherapy

Paxton V. Dickson,[1,5] John B. Hamner,[1,5] Thomas L. Sims,[1,5] Charles H. Fraga,[2] Catherine Y.C. Ng,[1] Surender Rajasekeran,[3] Nikolaus L. Hagedorn,[2] M. Beth McCarville,[4,6] Clinton F. Stewart,[2] and Andrew M. Davidoff[1,5]

Abstract

Purpose: Dysfunctional tumor vessels can be a significant barrier to effective cancer therapy. However, increasing evidence suggests that vascular endothelial growth factor (VEGF) inhibition can effect transient "normalization" of the tumor vasculature, thereby improving tumor perfusion and, consequently, delivery of systemic chemotherapy. We sought to examine temporal changes in tumor vascular function in response to the anti-VEGF antibody, bevacizumab.

Experimental Design: Established orthotopic neuroblastoma xenografts treated with bevacizumab were evaluated at serial time points for treatment-associated changes in intratumoral vascular physiology, penetration of systemically administered chemotherapy, and efficacy of combination therapy.

Results: After a single bevacizumab dose, a progressive decrease in tumor microvessel density to <30% of control was observed within 7 days. Assessment of the tumor microenvironment revealed a rapid, sustained decrease in both tumor vessel permeability and tumor interstitial fluid pressure, whereas intratumoral perfusion, as assessed by contrast-enhanced ultrasonography, was improved, although this latter change abated by 1 week. Intratumoral drug delivery mirrored these changes; penetration of chemotherapy was improved by as much as 81% when given 1 to 3 days after bevacizumab, compared with when both drugs were given concomitantly, or 7 days apart. Finally, administering topotecan to tumor-bearing mice 3 days after bevacizumab resulted in greater tumor growth inhibition (36% of control size) than with monotherapy (88% bevacizumab, 54% topotecan) or concomitant administration of the two drugs (44%).

Conclusions: Bevacizumab-mediated VEGF blockade effects alterations in tumor vessel physiology that allow improved delivery and efficacy of chemotherapy, although careful consideration of drug scheduling is required to optimize antitumor activity.

To grow beyond a few millimeters in size, solid tumors must develop an angiogenic phenotype that promotes the establishment of an expanding vascular network for delivery of oxygen and other nutrients (1). Vascular endothelial growth factor (VEGF) is well established as a central mediator in this process (2, 3). VEGF promotes endothelial cell proliferation, migration, and survival, as well as mobilization of marrow–derived endothelial precursors, in support of tumor angiogenesis, and is elaborated by both tumor and host cells in response to local environmental as well as intracellular stimuli. In addition, VEGF is a potent stimulator of vessel permeability, having originally been recognized for its function as a vascular permeability factor (4). Because of its fundamental role in tumor angiogenesis, VEGF serves as a logical target for antiangiogenic cancer therapy.

Bevacizumab is a humanized, monoclonal anti-VEGF antibody that neutralizes all isoforms of human VEGF (5). It is the first Food and Drug Administration–approved antiangiogenic agent for cancer therapy, based on its efficacy in combination with standard chemotherapy in patients with metastatic colorectal cancer (6). It is currently being investigated in clinical trials for patients with other locally advanced or metastatic cancers, with encouraging preliminary results (7). These clinical findings are consistent with a central, albeit somewhat counterintuitive, theme to emerge from several years of preclinical investigation of antiangiogenic therapies; these agents often have an additive or synergistic effect when used in

Authors' Affiliations: Departments of [1]Surgery, [2]Pharmaceutical Sciences, [3]Critical Care, and [4]Radiological Sciences, St. Jude Children's Research Hospital; and Departments of [5]Surgery and [6]Radiology, University of Tennessee-Memphis Health Science Center, Memphis, Tennessee

Received 2/2/07; revised 4/18/07; accepted 4/26/07.

Grant support: Alliance for Cancer Gene Therapy, the Assisi Foundation of Memphis, the USPHS Childhood Solid Tumor Program Project Grant CA23099, the Cancer Center Support Grant 21766 from the National Cancer Institute, and the American Lebanese Syrian Associated Charities.

The costs of publication of this article were defrayed in part by the payment of page charges. This article must therefore be hereby marked *advertisement* in accordance with 18 U.S.C. Section 1734 solely to indicate this fact.

Requests for reprints: Andrew M. Davidoff, Department of Surgery, St. Jude Children's Research Hospital, 332 North Lauderdale, Memphis, TN 38105. Phone: 901-495-4060; Fax: 901-495-2176; E-mail: andrew.davidoff@stjude.org.

doi:10.1158/1078-0432.CCR-07-0278

combination with traditional cytotoxic chemotherapy or ionizing radiation (8). One potential explanation for this synergy is that tumors are attacked on two fronts—cytotoxic agents are direct mediators of tumor cell death whereas antiangiogenic agents promote tumor cell death indirectly, by destroying the blood supply upon which tumors depend for progression. In addition, it has been shown that when administered with a frequent, low-dose schedule, certain chemotherapeutic drugs can have potent antiendothelial cell activity (9, 10). Conversely, evidence is accumulating that VEGF blockade, although traditionally presumed to exert direct activity only against the tumor endothelium, may also have direct antitumor effects against certain malignancies (11).

An alternative explanation for the apparent paradox of antitumor synergy between drugs that destroy the tumor vasculature and chemotherapeutics that require adequate tumor perfusion for delivery throughout a tumor mass has been hypothesized. Jain (12) has suggested that as antiangiogenic agents begin to restore a balance between proangiogenic and antiangiogenic cytokines, tumor vessels, at least transiently, display a structural and functional phenotype more reflective of normal blood vessels. Through this process, termed vascular "normalization," remodeled tumor vessels partially overcome the physiologic barriers to drug and oxygen delivery within tumors through an improvement in their functional efficiency, thus enhancing the delivery and, therefore, the antitumor activity of cytotoxic therapies. This process of vascular normalization seems to be transient, however, with a relatively narrow window during which synergy could likely be achieved, and after which time the tumor vasculature is destroyed.

Thus, although antiangiogenic agents may have the potential to enhance the efficacy of cytotoxic chemotherapy by increasing intratumoral drug penetration, these agents ultimately likely decrease blood flow and may negatively affect the delivery and efficacy of adjuvant therapy. Therefore, an understanding of the temporal changes in the tumor vasculature effected by these antiangiogenic agents is critical for guiding their scheduling, especially when being used in combination with cytotoxic chemotherapeutics, to maximize antitumor activity.

Numerous preclinical studies have shown that neuroblastoma is susceptible to antiangiogenic therapy (13–15), including anti-VEGF agents (16); therefore, drugs such as bevacizumab are currently being evaluated in ongoing clinical trials for children with neuroblastoma. However, no guidelines exist for the optimal scheduling and dosing of bevacizumab. In this study, we present preclinical studies of the phenotypic and functional effects of bevacizumab on the tumor vasculature in relevant orthotopic models of neuroblastoma, the results of which will assist in the rational design of clinical trials of this agent in children with neuroblastoma and, likely, other solid tumors.

Materials and Methods

Animal tumor model. The human neuroblastoma cell lines NB-1691 (provided by P. Houghton, Memphis, TN) and SK-N-AS (purchased from American Type Culture Collection) were used. Localized neuroblastoma xenografts were established by injection of 1.5×10^6 tumor cells into either the left retroperitoneum or s.c. space of 4- to 6-week-old male C.B-17 severe combined immunodeficient (SCID) mice, as previously described (17). Measurements of the s.c. tumors were made with calipers and measurements of retroperitoneum tumors were made by ultrasonography. One month after s.c. tumor cell injection, and 21 days after retroperitoneum tumor cell inoculation, tumors were generally ~200 to 400 mm^3. Animals treated with bevacizumab (Genentech) received 200 μg via tail vein injection. All murine experiments were done in accordance with a protocol approved by the Institutional Animal Care and Use Committee of St. Jude Children's Research Hospital.

Immunohistochemistry. Formalin-fixed, paraffin-embedded 4-μm-thick tumor sections were analyzed by immunohistochemical analysis for CD34 and α–smooth muscle actin immunoreactivity, as described previously, using rat anti-mouse CD34 (RAM 34, PharMingen) and mouse anti-human smooth muscle actin (clone 1A4, DAKO) antibodies (18). Sections were viewed and digitally photographed using an Olympus U-SPT light microscope with an attached charge coupled device camera. Four images at ×10 were taken of each tumor section with care to avoid areas of necrosis. Images were saved as JPEG files for further processing in Adobe Photoshop (Adobe Systems, Inc.). Positive staining was quantified using NIH image analysis software, Image J, and is reported as the mean number of positive pixels/tumor section. Total vessel length per tumor section was quantified for the CD34-stained sections using the method described by Wild (19). Serial sections were also stained with a rabbit anti-human Ki67 antibody (1:1,000, vector VP-K451) after heat-induced epitope retrieval in Target Retrieval Buffer (DAKO, S1699), and a terminal deoxyribonucleotide transferase–mediated nick-end labeling (TUNEL) assay was done using the Dead End kit (Promega, PRG7130) adapted for use on a DAKO Autostainer. Results are reported as the percentage of positive cells, with at least 2,000 nuclei being counted per section, with care being taken to avoid areas of necrosis.

Intravital microscopy. Mice bearing s.c. tumors were anesthetized with ketamine/xylazine (0.1 mL s.c.) and the skin overlying the tumors was opened to expose the tumors. The tumor vasculature was visualized using an industrial scale microscope (model MM-40, Nikon USA) with a digital camera (Photometric CoolSnap FX, Roper Scientific) and fluorescent (100 W mercury) light source. Images were acquired at ×40 magnification.

Evans blue dye assay. Vessel permeability was assessed using an Evans blue dye assay (20). One hundred microliters of 2% Evan's blue dye (MP Biomedicals) were administered via tail vein to tumor-bearing mice and allowed to circulate for 20 min. To remove remaining intravascular dye, mice were perfused with 10 mL of saline through the left ventricle with a right atrial vent. Tumors were then excised, divided into four to eight approximately equal-sized pieces, and weighed (no tumor section weighed >0.15 g). Each tumor section was then placed in 1 mL of formamide (Fisher Scientific) for 72 h for dye extraction. Tumor sections were then removed and the resultant extract was centrifuged. Levels of the dye were then quantified using a spectrophotometer at a wavelength of 620 nm. All samples were run in duplicate and compared with those of standards. The concentration of Evan's blue dye within a tumor (μg/g tumor tissue) was calculated by averaging the extraction values for each section from a tumor.

Tumor interstitial fluid pressure measurement. Tumor interstitial fluid pressure was determined in s.c. grown tumors using a needle pressure technique (21). A 23-gauge hollow bore needle with an additional side hole cut 5 mm from the tip was connected to saline-filled tubing. This was connected via a fluid-filled dome diaphragm (Memscap AS) to a MLT844 physiologic pressure (AD Instruments, North America). All bubbles were carefully expelled from the system. The transducer was connected to a ML110 bridge amplifier (AD Instruments, North America) and data were imported into PowerLab software (AD instruments, North America). Before and in between recordings of individual tumor pressures, the system was calibrated using a graduated water column. Data are reported in mm Hg (1 cm H_2O = 1.36 mm Hg).

Contrast-enhanced ultrasonography. Ultrasonography was done with an Acuson Sequoia ultrasound machine (Siemens) using a

15L8 MHz transducer. For evaluation of contrast agent flow, tumors were imaged in the transverse plane in the region with the largest dimensions. The machine's mechanical index was lowered to ≤0.4 to prevent microbubble destruction. Optison ultrasound contrast agent (Amersham Health, Inc.), a suspension of human serum albumin microspheres encapsulating octafluoropropane gas, was used as the contrast agent. Mean microsphere size of Optison ranges from 2 to 4.5 μm and the particles remain in the intravascular space. A 27-gauge needle was used to give bolus injections of 0.1 mL of Optison diluted in 0.1 mL of saline, via a tail vein. Images were recorded on cine clips starting immediately before the injection and continuing for 30 s, at a frame rate of 30 to 70 Hz. The clips were later analyzed on-line using the Cadence contrast pulse sequence ACQ software (Siemens). A region of interest was drawn to encompass the entire tumor and the software determined the average log-compressed signal intensity within the region of interest for each image frame over the 30-s imaging period.

Intratumoral drug penetration. Animals treated with topotecan (GlaxoSmithKline) received 1 mg/kg via tail vein injection. One hour after this bolus topotecan administration, whole blood (in EDTA) and tumor tissue were collected. Tumors were snap frozen in liquid nitrogen before being homogenized in PBS (100 μL/mg tissue) and centrifuged to remove particulates. Cold methanol (4:1) was added to the supernatant, and the plasma was collected from the whole blood, to extract the topotecan. Samples were centrifuged and the methanolic supernatant was stored at -80°C until analysis. The extracted tumor and plasma samples were converted to total topotecan by adding five parts methanolic supernatant to one part 20% phosphoric acid. The methanolic supernatant from tumor tissue or plasma was analyzed for topotecan by an isocratic high-performance liquid chromatography with fluorescence detection (RF10AXL; Shimadzu); the excitation and emission wavelengths were 370 and 530 nm, respectively (22).

Animals treated with etoposide (Pfizer) received 375 μg via tail vein injection. As above, 1 h later, whole blood (in EDTA) and tumor tissue were collected for quantitation of etoposide concentrations. To prevent degradation of etoposide by oxidation, 1 μL of 2 mol/L ascorbic acid in PBS was added for every 100 μL of blood, immediately after it was collected. Samples were centrifuged and the plasma was isolated, frozen on dry ice, and stored at -80°C until extracted and analyzed. Tumors were weighed and snap frozen in liquid nitrogen. The tumors were then homogenized in PBS (100 μL/mg tissue) containing 20 μmol/L ascorbic acid and centrifuged to remove particulates. The etoposide-containing supernatant was removed and stored at -80°C until extracted using a previously reported method (23). The reconstituted tumor and plasma extracts were analyzed for etoposide using a modification of a previously reported high-performance liquid chromatography with electrochemical detection method (Coulochem II with Model 5010 dual electrode analytic cell; Environmental Sciences Association; ref. 23). Etoposide catechol was not measured in these experiments; therefore, the organic component of the mobile phase was increased to shorten the retention time of etoposide to 5.5 min [60% 25 mmol/L citric acid – 50 mmol/L sodium phosphate (pH 2.4) – 40% acetonitrile].

Statistical analysis. Results are reported as mean ± SE. The Sigmaplot program (SPSS, Inc.) was used to analyze and graphically present the data. An unpaired Student's *t* test was used to analyze statistical differences in the results. All *P* values are reported in the figure legends.

Results

Bevacizumab rapidly alters the morphology of the tumor vasculature in treated neuroblastoma xenografts. We first examined the effect of VEGF inhibition on microvessel density, pericyte coverage, vessel length, and tumor vessel phenotype at 24 h, 3 days, and 7 days after administration of a single dose of bevacizumab to mice with established, orthotopic NB-1691 xenografts. Tumors from cohorts of mice sacrificed at each of these time points showed a significant, rapid, and progressive decrease (<50% of control by day 1, <30% by day 7) in tumor microvessel density, as assessed by CD34 immunohistochemistry, in bevacizumab-treated tumors, compared with control-treated tumors, in which microvessel density did not change significantly over time with tumor growth (Fig. 1A and B). Serial tumor sections were also stained for smooth muscle actin to identify perivascular smooth muscle cells. This revealed a paucity of these stabilizing perivascular cells in untreated neuroblastoma xenografts, as often occurs in the neovessels of solid tumors (24). This remained unchanged after bevacizumab treatment (data not shown). Thus, unlike the marked loss of endothelial cells in treated tumors, the number of pericytes remained stable, resulting in an effective increase in the vessel maturity index (ratio of pericytes to endothelial cells) of the intratumoral vessels (Fig. 1B). This suggests that there was a selective loss of the more immature vessels that lacked pericytes, whereas the more mature vessels remained. Vessel length also rapidly and progressively declined in treated tumors, being <25% of control tumors by day 7 after bevacizumab administration (Fig. 1B). Interestingly, despite the reduction in tumor microvessel density, there was a relative lack of necrosis within sections of bevacizumab-treated tumors compared with controls (Fig. 1C).

To further examine morphologic alterations of the tumor vasculature with bevacizumab treatment, we used intravital microscopy for *in vivo* analysis of acute tumor preparations. These images showed dramatic qualitative differences in tumor vessel architecture after treatment. Vessels within control tumors were chaotic and dilated, with abrupt changes in vessel diameter and direction. During bevacizumab-induced vessel regression, the vessels that remained had a more normal structural phenotype, similar to that seen in the vessels within normal skin (Fig. 2).

Finally, in a separate cohort of mice, we examined the effect of VEGF inhibition with bevacizumab on the growth of established NB-1691 xenografts. Three weeks after tumor cell inoculation, when retroperitoneal tumors were ~600 mm^3, mice were treated with a single i.v. dose of bevacizumab (200 μg) or saline (control). Tumor volume was then serially assessed by transabdominal ultrasound (Fig. 3). Interestingly, despite the profound histologic changes observed in the tumor vasculature after a single dose of bevacizumab previously noted, tumor growth in treated mice was not significantly different from that of controls, with little inhibition of tumor growth observed at day 7 after the bevacizumab dose (mean bevacizumab-treated tumor volume 3,256 ± 470 mm^3, mean control tumor volume 3,463 ± 422 mm^3).

Improvement in intratumoral vessel function with bevacizumab. As previously mentioned, one of the most profound characteristics of VEGF is its ability to act as a potent stimulator of vessel permeability (4). To examine the effect of bevacizumab on vessel permeability in our model of neuroblastoma, we compared the extravasation of Evan's blue dye into the parenchyma of treated tumors, with control tumors, and found that bevacizumab treatment induced a rapid and sustained decrease in tumor vessel permeability. At 24 h, 3 days, and 7 days after treatment, Evan's blue dye extravasation into tumors of bevacizumab-treated mice was reduced to 62.2 ± 2.4%, 33.9 ± 2.6%, and 51.8 ± 8.0%, respectively, the degree of

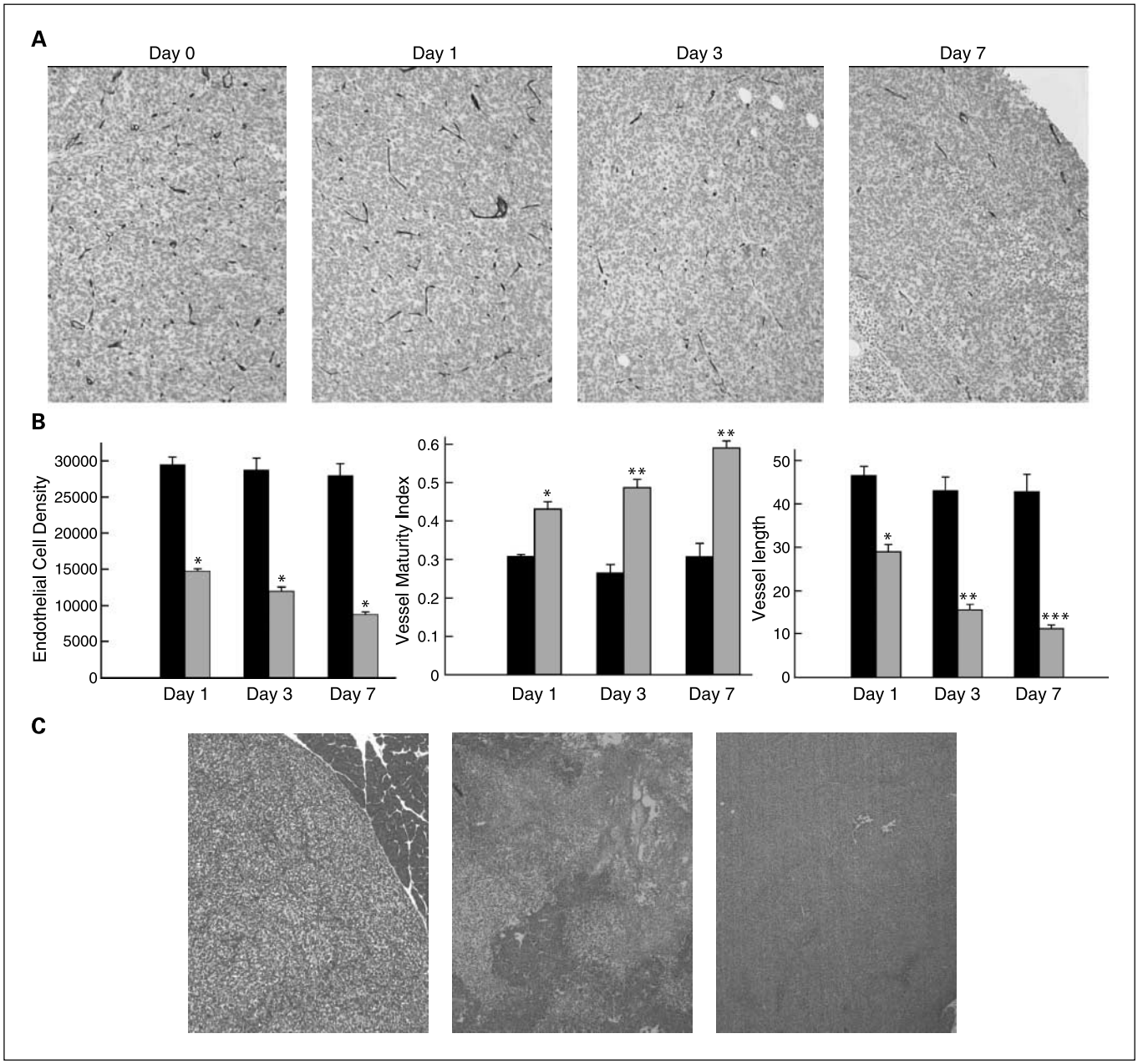

Fig. 1. The effect of a single dose of bevacizumab on the histology of tumor vessels within established retroperitoneal NB-1691 xenografts. *A,* representative CD34 immunohistochemistry at days 0, 1, 3, and 7 after bevacizumab administration. Original magnification, ×10. Quantitation of the (*B*) endothelial cell density (mean CD34 pixel count/tumor section, $^*P < 0.001$ at each time point), vessel maturity index (ratio of α – smooth muscle actin to CD34 pixels per tumor section; *, $P = 0.003$ at day 1; **, $P < 0.001$ at days 3 and 7), and vessel length (mean vessel length in pixels/tumor section; *, $P = 0.006$, day 1; **, $P = 0.007$, day 3; ***, $P = 0.004$, day 7) within bevacizumab-treated (*gray columns*) and control-treated tumors (*black columns*; $n = 5$/group). *C,* representative H&E sections from a tumor at day 0 (*left*, note the normal adrenal gland is still identifiable in the top right corner), and control-treated (*middle*) and bevacizumab-treated (*right*) tumors 7 d after treatment, highlighting the absence of necrosis in the bevacizumab-treated tumors. Original magnification, ×10.

Evan's blue dye extravasation in size-matched controls at each time point (Fig. 4A). We next investigated how bevacizumab-induced reduction in tumor vessel permeability would affect tumor interstitial fluid pressure. A reduction in interstitial fluid pressure was observed; at 24 h, 3 days, and 7 days after treatment, tumor interstitial fluid pressure was reduced to 44% (5.33 ± 1.24 versus 12.13 ± 0.93 mm Hg), 40% (4.40 ± 0.42 versus 10.87 ± 0.50 mm Hg), and 40% (4.65 ± 0.95 versus 11.67 ± 0.69 mm Hg), respectively, the tumor interstitial fluid pressure of size matched controls at each time point (Fig. 4A).

We next did quantitative contrast-enhanced ultrasonography to evaluate how these alterations in tumor vessel structure and function affected tumor perfusion. We have previously shown that measuring intratumoral flow of an ultrasound microbubble contrast agent, as assessed by the change in signal intensity (ΔSI) after i.v. injection of the agent, is a reliable method for monitoring tumor vascular response to antiangiogenic therapy (25). Using this modality, we compared tumor perfusion in bevacizumab- and control-treated mice with size-matched retroperitoneal tumors. Interestingly, the ΔSI in

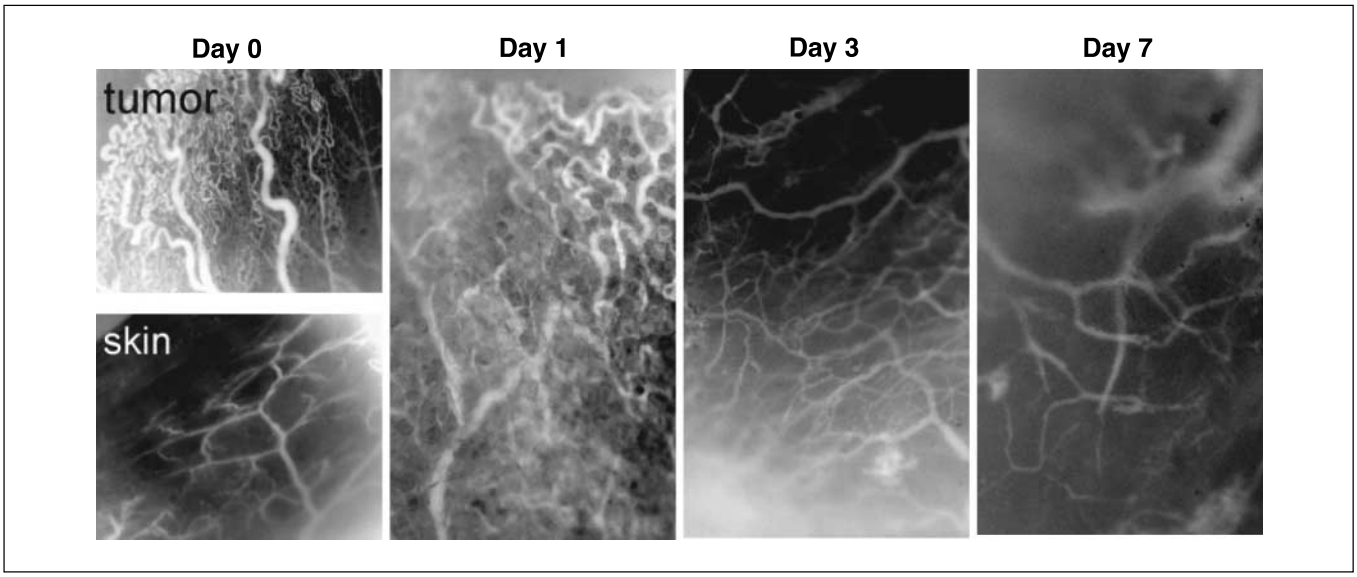

Fig. 2. The effect of a single dose of bevacizumab on the intratumoral vascular phenotype within established NB-1691 xenografts, as assessed by intravital microscopy at days 0, 1, 3, and 7. Original magnification, ×40. Shown also is the vasculature of normal skin.

bevacizumab-treated tumors was increased by 30.6% (17.38 ± 0.99 dB versus 13.30 ± 0.73 dB) by 24 h and 45.5% (14.25 ± 1.40 dB versus 9.29 ± 1.15 dB) at day 3, versus size-matched controls (Fig. 4A). Moreover, within bevacizumab-treated tumors, contrast enhancement was more homogenous throughout the tumor mass compared with controls where enhancement was largely restricted to the tumor periphery (Fig. 4B). At day 7, however, this measure of tumor perfusion was nearly equivalent for bevacizumab- and control-treated tumors (9.66 ± 0.24 dB versus 9.68 ± 0.69 dB), highlighting the transient nature of the change in intratumoral perfusion. Considering the significant vessel regression occurring in the tumors of bevacizumab-treated mice, as judged by immunohistochemical analyses, these findings suggest that the mature vessels that remain in the first few days after bevacizumab administration permit more efficient tumor perfusion compared with the highly disorganized vasculature within controls.

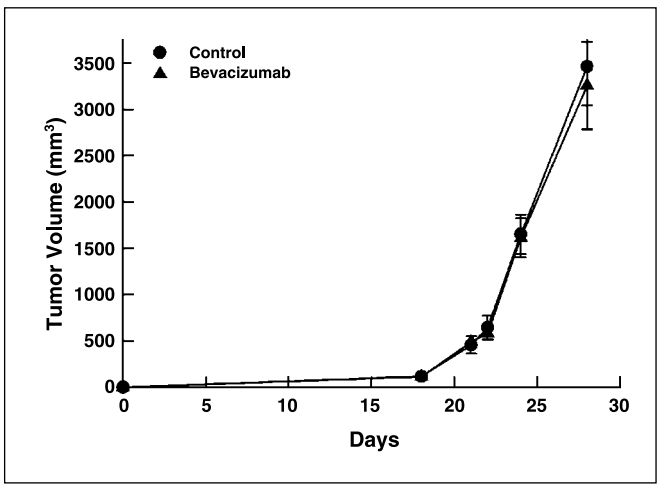

Fig. 3. Growth of established NB-1691 xenografts after the administration of a single dose of bevacizumab at day 21 after tumor cell inoculation (n = 5/group, P = 0.75 at day 28).

Consistent with this demonstration of improved intratumoral perfusion, in addition to the diminished degree of frank necrosis, we observed a significant decrease in the TUNEL positivity of bevacizumab-treated tumors, compared with controls (1.6 ± 0.1% versus 12.2 ± 4.5%) and a trend toward increased Ki-67-positivity (51.6 ± 1.9% versus 47.6 ± 1.5%) 1 day after treatment (Fig. 4C). This effect abated by day 3, however.

Bevacizumab improves tumor penetration of systemically administered chemotherapy. We next evaluated how these alterations in tumor vessel structure and function would effect tumor penetration of systemically administered chemotherapeutic agents. Mice with established retroperitoneal NB-1691 xenografts were given a single i.v. dose of bevacizumab (200 μg) or saline (control) 21 days after tumor cell inoculation when tumors were ~400 mm^3. Subsequently, these mice received a single i.v. dose of topotecan (2 mg/kg) either concurrent with, 24 h after, 3 days after, or 7 days after administration of the dose of bevacizumab (or vehicle control). Although each mouse received the same topotecan dose, tumor topotecan penetration was determined as the ratio of the concentration of topotecan within the tumor to that in the plasma, to account for fluctuations in plasma topotecan concentrations. Analysis revealed that tumor topotecan penetration remained relatively stable in control-treated mice for each successive time point. However, in mice treated with bevacizumab, intratumoral drug penetration was found to increase progressively compared with size-matched controls, when topotecan was administered at 24 h (51% versus 43%) and 3 days (57% versus 34%) after bevacizumab. However, this improvement in penetration was no longer seen at day 7 (39% versus 40%), similar to the results previously detailed for the transient change in intratumoral perfusion effected by a single dose of bevacizumab (Fig. 5A).

To determine whether this phenomenon of improved intratumoral drug delivery occurred broadly, we did similar

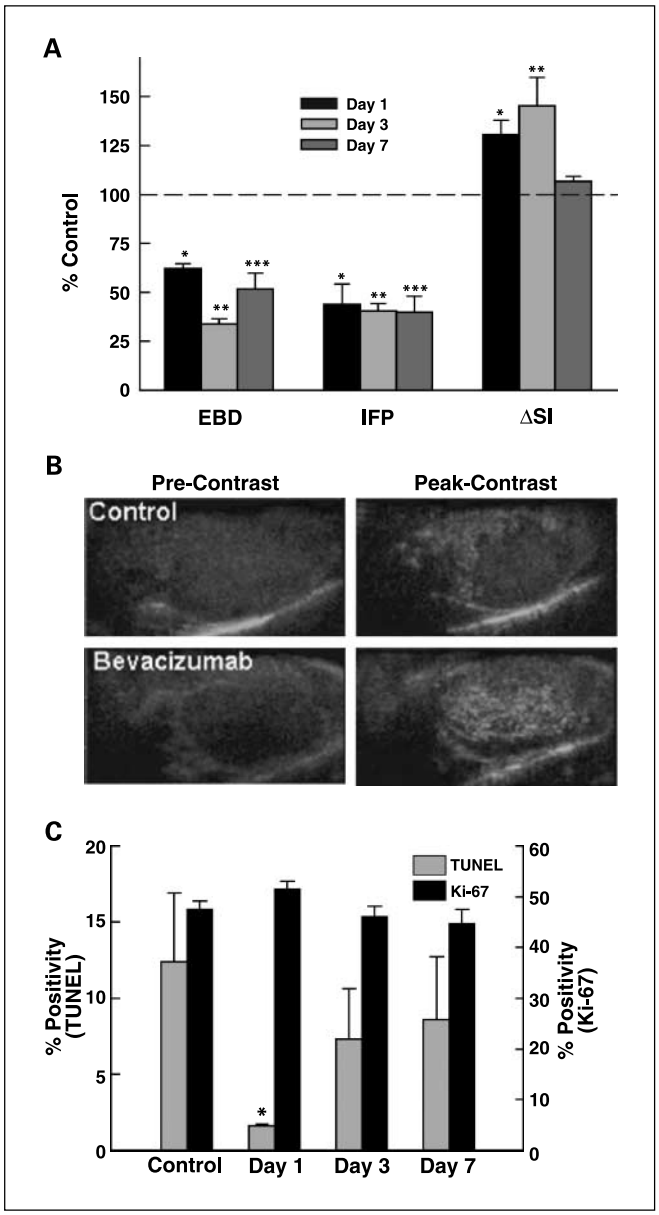

Fig. 4. The effect of a single dose of bevacizumab on the function of the intratumoral vasculature within established retroperitoneal NB-1691 xenografts, compared with size-matched control-treated tumors. *A,* assessment, with five mice per group, included vessel permeability, as determined by Evan's blue dye (*EBD*) extravasation (*, $P = 0.02$, day 1; **, $P = 0.003$, day 3; ***, $P = 0.03$, day 7), interstitial fluid pressure (*IFP*) within tumors (*, $P = 0.01$, day 1; **, $P = 0.001$, day 3; ***, $P = 0.004$, day 7), and intratumoral perfusion, as determined by contrast-enhanced ultrasonography (change in signal intensity, ΔSI) studies (*, $P = 0.01$, day 1; **, $P = 0.03$, day 3; $P = 0.92$, day 7). *B,* representative contrast-enhanced ultrasound images of bevacizumab- and control-treated tumors before and after i.v. contrast administration. *C,* the percentage of cells in tumor sections that were TUNEL positive (*gray columns*) and Ki-67 positive (*black columns*) 1, 3, and 7 d after tumor-bearing mice received a single dose of bevacizumab (*$P = 0.05$, day 1; $P = 0.48$, day 3; $P = 0.60$, day 7 for TUNEL and $P = 0.16$, day 1; $P = 0.58$, day 3; $P = 0.39$, day 7 for Ki-67, compared with control).

experiments in which a different chemotherapeutic agent (etoposide) was administered and where a different tumor cell line (SK-N-AS) was used as an alternate orthotopic neuroblastoma xenograft. Etoposide was chosen for study because of its different physicochemical properties from topotecan, specifically, being more lipophilic and highly protein bound than the water-soluble topotecan. SK-N-AS was chosen because unlike most neuroblastoma cell lines, it does not have an amplified number of copies of the *MYCN* oncogene. Although the results were not identical to what had been found in our initial experiments with topotecan using the NB-1691 cell line, improvement in intratumoral drug penetration was noted when the chemotherapeutic drug was administered 24 h and 3 days after a bevacizumab dose. For etoposide given to mice

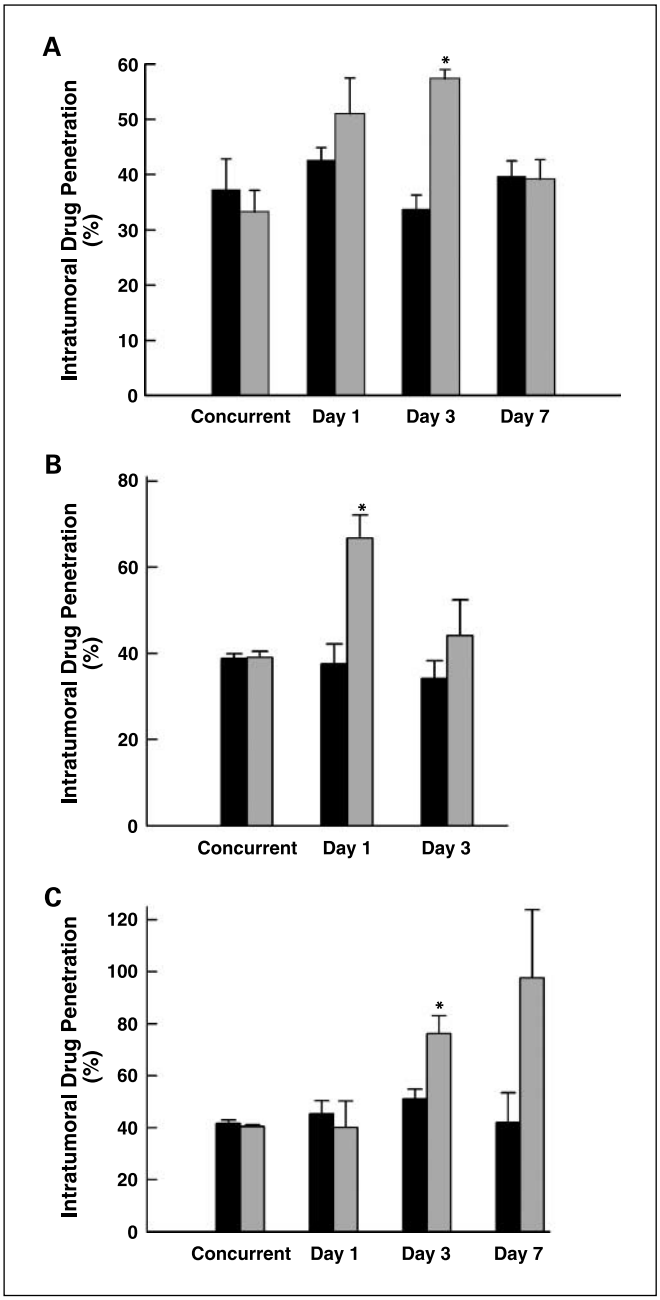

Fig. 5. The effect of bevacizumab on the intratumoral penetration of systemically administered chemotherapy when delivered at different days after the bevacizumab dose in mice bearing established retroperitoneal neuroblastoma xenografts ($n = 4$/group). *A,* topotecan penetration in NB-1691 xenografts ($P = 0.57$, day 0; $P = 0.22$, day 1; *, $P < 0.001$, day 3; $P = 0.91$, day 7). *B,* etoposide penetration in NB-1691 xenografts ($P = 0.64$, day 0, *, $P = 0.005$, day 1; $P = 0.28$, day 3). *C,* topotecan penetration in SK-N-AS xenografts ($P = 0.55$, day 0; $P = 0.64$, day 1; *, $P = 0.007$, day 3; $P = 0.23$, day 7). Black columns, control-treated tumors; gray columns, bevacizumab-treated tumors.

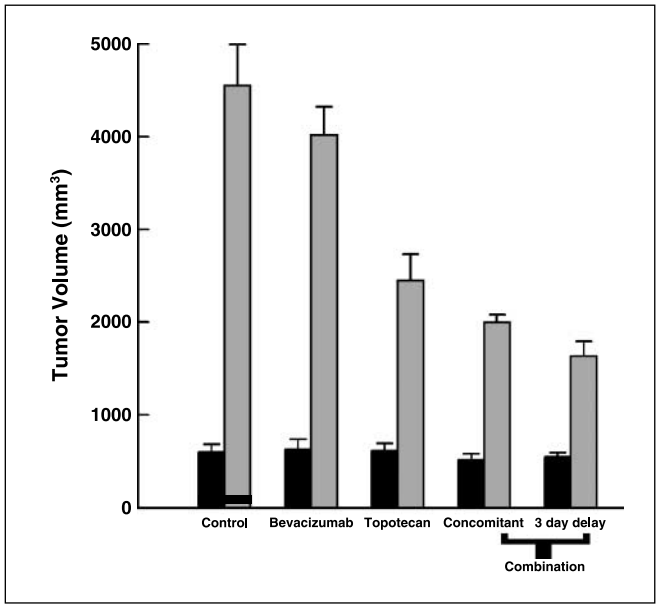

Fig. 6. The effect on the growth of established NB-1691 retroperitoneal tumors treated at day 21 (size matched by ultrasonographic measurement, *black columns*) after tumor cell injection with either vehicle control, a single dose of bevacizumab or topotecan, or the combination of bevacizumab and topotecan given either concomitantly or when the topotecan dose followed the bevacizumab dose by 3 d (n = 7/group). Tumor volumes were measured at day 28 (*gray columns*, *, P = 0.01, comparing the final tumor volume in mice treated with topotecan 3 d after bevacizumab with mice that received topotecan alone; P = 0.17, comparing the final tumor volume in mice treated with topotecan 3 d after bevacizumab with mice that received both drugs concomitantly; P = 0.27, comparing the final tumor volume in mice treated with topotecan alone with mice that received both topotecan and bevacizumab concomitantly).

with NB-1691 xenografts treated with bevacizumab, the percent intratumoral drug penetration was 67% at day 1 compared with 37% in control-treated tumors, a 1.8-fold increase. By day 3, however, this improvement had already declined to only a 1.3-fold increase over control (44% versus 33%; Fig. 5B). When topotecan was given to mice with SK-N-AS xenografts treated with bevacizumab, the percent intratumoral drug penetration at day 1 was not significantly different from control-treated tumors (40% versus 43%). However, at day 3, intratumoral drug penetration in bevacizumab-treated tumors was significantly improved (75% versus 50%, a 1.5-fold increase; Fig. 5C). Interestingly, the day 7 data revealed a greater improvement in intratumoral topotecan penetration in mice that received a dose of bevacizumab (whereas that in control-treated mice remained stable); however, because of variability in the data, these results did not reach statistical significance.

Bevacizumab improves efficacy of systemically administered topotecan. Finally, we examined the therapeutic consequence of improved tumor drug penetration achieved after pretreatment with a single bevacizumab dose. Again, retroperitoneal NB-1691 xenografts were established and, 21 days later, tumor-bearing mice were divided into five groups with size-matched tumors. Group 1 served as control; group 2 received a single dose of bevacizumab on day 21; group 3 received a single dose of topotecan on day 21; group 4 received a single dose of both bevacizumab and topotecan on day 21 (concomitant); and group 5 received the dose of bevacizumab on day 21 followed by topotecan on day 24 (3-day delay). All animals were sacrificed on day 28 and assessed for tumor size. As seen previously, a single dose of bevacizumab had only a modest effect on tumor growth [88% of control, final tumor volume 4,020 ± 302 mm^3 versus 4,556 ± 439 mm^3 (control)]. Topotecan monotherapy did affect significant tumor growth inhibition compared with controls (54% of control, final volume 2,454 ± 279 mm^3). The antitumor effect of topotecan was improved when given together with bevacizumab (44% of control, final volume 1,999 ± 350 mm^3). However, when topotecan was administered 3 days after treatment with bevacizumab, this combination had an even more pronounced effect (36% of control, final volume 1,639 ± 244 mm^3) although the difference did not reach statistical significance when compared with concomitant administration of the two drugs (Fig. 6).

Discussion

In this study, we have shown the functional changes that occur as a result of the remodeling of tumor vasculature with bevacizumab in a relevant, orthotopic model of neuroblastoma. Although the importance of normalization of the intratumoral vasculature is becoming increasingly appreciated (26), this is the first study to show that this normalization has functional consequences with regard to the intratumoral delivery and antitumor activity of adjuvant anticancer agents when given together with bevacizumab. Our results also show that the antitumor effect depends, at least in part, on drug scheduling.

The aberrant structure and function of tumor neovessels leads to a microenvironment within solid tumors that is characterized by elevated interstitial fluid pressure, inefficient tumor perfusion, and significant areas of hypoxia and acidosis (27, 28). These factors contribute to poor intratumoral drug delivery and activity, and, in part, to the development of resistance to cytotoxic therapies. We have shown that inhibition of tumor elaborated VEGF with bevacizumab effects a transient remodeling of the intratumoral vasculature, which, despite causing an overall decrease in intratumoral microvessel density, results in more efficient perfusion of tumors in mice with established, orthotopic neuroblastoma xenografts. This remodeling of the vasculature to a more mature, functional phenotype seems to have been achieved by destroying the immature vessels in which the endothelial cells lack the support of adjacent pericytes. Vessels composed of endothelial cells invested with pericytes are likely able to survive because the critical endothelial cell survival factor, VEGF, is delivered in a paracrine manner by these support cells. This process of evolving a more mature vasculature by pruning away immature vessels is in distinction to that observed during treatment of glioblastoma xenografts (29) and murine mammary carcinomas (30) with DC101, a VEGFR2 blocking antibody, in which an increase in the ratio of Ang-1/Ang-2 elaborated by the tumor cells seems to cause an active recruitment of pericytes to immature tumor vessels. We detected no significant change in Ang-1 or Ang-2 expression in our bevacizumab-treated xenografts (data not shown).

We have shown that one of the consequences of remodeling the intratumoral vasculature with bevacizumab is an associated improvement in intratumoral penetration of systemic chemotherapy. The reasons for this are likely multifactorial. One relates to the effect of bevacizumab on tumor interstitial pressure. Tumor vessel hyperpermeability leads to leaking of

plasma proteins and fluid into the tumor interstitium, resulting in a marked elevation in tumor interstitial pressures (31, 32). Moreover, solid tumors lack functional lymphatics, and therefore have little means to remove the excess interstitial fluid (28, 31). As a result, there is near equilibration between the hydrostatic and oncotic pressure gradients that normally exist between the intravascular and interstitial compartments. Consequently, forces that ordinarily govern the transport of fluid and molecules across a microvascular bed are significantly impaired. VEGF, a known vascular permeability factor, contributes significantly to tumor vessel leakiness through a variety of proposed mechanisms (33). Conversely, VEGF inhibition can reduce tumor vessel permeability, lower tumor interstitial pressures, and, in turn, begin to restore transvascular pressure gradients that improve tumor drug penetration (30–35). Consistent with this, we observed that administration of a single dose of bevacizumab to mice bearing neuroblastoma xenografts resulted in a rapid and sustained decrease in tumor vessel permeability and interstitial pressure compared with mice with size-matched control tumors, and coincident improvement in intratumoral drug delivery. These data are also consistent with other xenograft models (30, 36) and recent data from patients with locally advanced rectal cancer (37).

In addition to elevated interstitial pressures and altered transcapillary pressure gradients, another factor contributing to poor tumor drug delivery is inefficient tumor blood flow due to both the heterogeneous distribution of vessels throughout a tumor mass, as well as physical resistance to perfusion of these chaotic vessels (38, 39). Although it might be expected that antiangiogenic therapy and tumor vessel regression would result in a decrease in tumor perfusion, the converse often occurs. For example, Wildiers et al. (35) quantified tumor perfusion in s.c. grown HT29 tumors using the fluorescent dye H33342 and found that after treatment with anti-VEGF antibody, there was actually an increase in global perfusion of treated mice versus controls. Similarly, in our experiments, we found that 24 h and 3 days after treatment, tumor perfusion was significantly improved in mice that had received bevacizumab compared with that of controls. Importantly, this effect was transient, being lost at 7 days when there was equal tumor perfusion between the groups. The loss of this effect is not likely due to clearance of the antibody that has a long half-life (approximately 20 days). Given that bevacizumab was found to cause a significant decrease in the number of tumor vessels, these findings suggest that the remaining vessels allow much more efficient blood flow. It is likely that this improved perfusion efficiency is due, at least in part, to the decreased resistance to flow within these vessels, as it has been shown that excessive and chaotic branching within tumor vessels contributes to increased resistance to tumor circulation (39). As revealed with intravital microscopy, the vessels that remain within tumors after treatment with bevacizumab have an ordered structure much more reflective of those within in normal tissue, compared with the disorganized vessels seen in control tumors. In addition, the reduction of tumor interstitial pressure described previously, together with improved support from investing pericytes, may result in fewer areas of collapse of intratumoral vessels that tend to be compressed due both to the high tumor interstitial fluid pressure and the expanding tumor mass.

The important clinical implication of normalizing the tumor vasculature during anti-VEGF therapy is improved delivery of chemotherapeutic agents to a tumor mass. Our data are in agreement with accumulating evidence that show that manipulation of the tumor vasculature and microenvironment may indeed improve tumor drug delivery (21, 35, 40). However, fundamental to achieving this effect is defining the appropriate schedule for administering antiangiogenic and cytotoxic agents. Although concurrent administration of chemotherapy with bevacizumab has shown efficacy in clinical trials, it may be that the effectiveness of this combination can be improved with an alternative dosing schedule. In the current study, tumor penetration of systemically administered topotecan was not significantly altered when given at the same time as bevacizumab. However, when administered at later time points after bevacizumab, a progressive increase in tumor topotecan penetration was observed, which was significant by day 3. However, when injected 7 days after bevacizumab, tumor drug penetration decreased to the level of controls, highlighting the transient nature of this phenomenon. These findings are consistent with the hypothesis that tumor vasculature normalization with anti-VEGF therapy provides a ''window'' for optimizing the effects of adjuvant cytotoxic therapy (26). Although the normalized vasculature is more efficient and, initially, permits improved perfusion and drug delivery, it seems that the beneficial alterations in tumor vessel physiology may ultimately be balanced by the progressive reduction in vessel number.

Thus, in the current investigation, we have shown significant changes in tumor vessel morphology and function in mice bearing human neuroblastoma xenografts in response to inhibition of VEGF. These changes result in improved delivery and activity of systemically administered chemotherapy, demonstrating that pharmacologic manipulation of the tumor vasculature can be used to improve the antitumor efficacy of adjuvant therapy. It is uncertain whether this ''window of opportunity'' will be the same when trying to achieve synergy with different antiangiogenic agents and chemotherapetuics with different physicochemical properties against different types of solid tumors. We did note differences in the kinetics of the changes in vascular physiology when using a different tumor cell line and when trying to deliver a different chemotherapeutic agent. It is also unclear how the findings in our murine model will translate into humans, particularly given the inability of bevacizumab to inhibit murine VEGF. Nevertheless, our study does show feasibility of overcoming some of the barriers to successful chemotherapy by improving the intratumoral delivery and efficacy of systemic chemotherapy. Thus, as antiangiogenic agents continue to move forward into clinical trials, appropriate patient selection, as well as the dose and scheduling of angiogenesis inhibitors and cytotoxic agents, will need to be carefully considered to optimize the efficacy of combination therapies.

Acknowledgments

We thank Dorothy Bush for her assistance with immunohistochemistry, Stacey Glass for her assistance with ultrasonography, and Dr. Victor Santana for his critical review of the manuscript.

References

1. Folkman J. Fundamental concepts of the angiogenic process. Curr Mol Med 2003;3:643–51.
2. Hicklin DJ, Ellis LM. Role of the vascular endothelial growth factor pathway in tumor growth and angiogenesis. J Clin Oncol 2005;23:1011–27.
3. Ferrara N, Gerber HP, LeCouter J. The biology of VEGF and its receptors. Nat Med 2003;9:669–76.
4. Senger DR, Galli SJ, Dvorak AM, et al. Tumor cells secrete a vascular permeability factor that promotes accumulation of ascites fluid. Science 1983;219:983–5.
5. Gerber HP, Ferrara N. Pharmacology and pharmacodynamics of bevacizumab as monotherapy or in combination with cytotoxic therapy in preclinical studies. Cancer Res 2005;65:671–80.
6. Hurwitz H, Fehrenbacher L, Novotny W, et al. Bevacizumab plus irinotecan, fluorouracil, and leucovorin for metastatic colorectal cancer. N Engl J Med 2004; 350:2335–42.
7. Johnson DH, Fehrenbacher L, Novotny WF, et al. Randomized phase II trial comparing bevacizumab plus carboplatin and paclitaxel with carboplatin and paclitaxel alone in previously untreated locally advanced or metastatic non-small-cell lung cancer. J Clin Oncol 2004;22:2184–91.
8. Gasparini G, Longo R, Fanelli M, Teicher BA. Combination of antiangiogenic therapy with other anticancer therapies: results, challenges, and open questions. J Clin Oncol 2005;23:1295–311.
9. Browder T, Butterfield CE, Kraling BM, et al. Antiangiogenic scheduling of chemotherapy improves efficacy against experimental drug-resistant cancer. Cancer Res 2000;60:1878–86.
10. Kerbel RS, Kamen BA. The anti-angiogenic basis of metronomic chemotherapy. Nat Rev Cancer 2004;4: 423–36.
11. Fakhari M, Pullirsch D, Abraham D, et al. Selective upregulation of vacular endothelial growth factor receptors neuropilin-1 and -2 in human neuroblastoma. Cancer 2002;94:258–63.
12. Jain RK. Normalizing tumor vasculature with anti-angiogenic therapy: a new paradigm for combination therapy. Nat Med 2001;7:987–9.
13. Crawford SE, Stellmach V, Ranalli M, et al. Pigment epithelium-derived factor (PEDF) in neuroblastoma: a multifunctional mediator of Schwann cell antitumor activity. J Cell Sci 2001;114:4421–8.
14. Streck CJ, Ng CY, Zhang Y, et al. Interferon-mediated anti-angiogenic therapy for neuroblastoma. Cancer Lett 2005;228:163–70.
15. Shusterman S, Grupp SA, Barr R, et al. The angiogenesis inhibitor tnp-470 effectively inhibits human neuroblastoma xenograft growth, especially in the setting of subclinical disease. Clin Cancer Res 2001; 7:977–84.
16. Kim ES, Serur A, Huang J, et al. Potent VEGF blockade causes regression of coopted vessels in a model of neuroblastoma. Proc Natl Acad Sci U S A 2002;99: 11399–404.
17. Streck CJ, Zhang Y, Miyamoto R, et al. Restriction of neuroblastoma angiogenesis and growth by interferon-α/β. Surgery 2004;136:183–9.
18. Spurbeck WW, Ng CY, Strom TS, Vanin EF, Davidoff AM. Enforced expression of tissue inhibitor of matrix metalloproteinase-3 affects functional capillary morphogenesis and inhibits tumor growth in a murine tumor model. Blood 2002;100:3361–8.
19. Wild R, Ramakrishnan S, Sedgewick J, Griffioen AW. Quantitative assessment of angiogenesis and tumor vessel architecture by computer-assisted digital image analysis: effects of VEGF-toxin conjugate on tumor microvessel density. Microvasc Res 2000;59: 368–76.
20. Farrell C, Stewart P, Del Maestro R. A new glioma model in rat: the C6 spheroid implantation technique permeablility and vascular characterization. J Neurooncol 1987;4:403–15.
21. Pietras K, Rubin K, Sjoblom T, et al. Inhibition of PDGF receptor signaling in tumor stroma enhances antitumor effect of chemotherapy. Cancer Res 2002; 62:5476–84.
22. Zamboni WC, Stewart CF, Thompson J, et al. Relationship between topotecan systemic exposure and tumor response in human neuroblastoma xenografts. J Natl Cancer Inst 1998;90:505–11.
23. Cai X, Woo M, Edick M, Relling M. Simultaneous quantitation of etoposide and its catechol metabolite in human plasma using high-performance liquid chromatography with electrochemical detection. J Chromatogr B 1999;728:241–50.
24. Morikawa S, Baluk P, Kaidoh T, et al. Abnormalities in pericytes on blood vessels and endothelial sprouts in tumors. Am J Pathol 2002;160:985–1000.
25. McCarville MB, Streck CJ, Dickson PV, et al. Angiogenesis inhibitors in a murine neuroblastoma model: quantitative assessment of intratumoral blood flow with contrast-enhanced gray-scale US. Radiology 2006;240:73–81.
26. Jain RK. Normalization of tumor vasculature: an emerging concept in antiangiogenic therapy. Science 2005;307:58–62.
27. Hagendoorn J, Tong R, Fukumura D, et al. Onset of abnormal blood and lymphatic vessel function and interstitial hypertension in early stages of carcinogenesis. Cancer Res 2006;66:3360–4.
28. Cairns R, Papandreou I, Denko N. Overcoming physiologic barriers to cancer treatment by molecularly targeting the tumor microenvironment. Mol Cancer Res 2006;4:61–70.
29. Winkler F, Kozin SV, Tong RT, et al. Kinetics of vascular normalization by VEGFR2 blockade governs brain tumor response to radiation: role of oxygenation, angiopoietin-1, and matrix metalloproteinases. Cancer Cell 2004;6:553–63.
30. Tong RT, Boucher Y, Kozin SV, et al. Vascular normalization by vascular endothelial growth factor receptor 2 blockade induces a pressure gradient across the vasculature and improves drug penetration in tumors. Cancer Res 2004;64:3731–6.
31. Heldin CH, Rubin K, Pietras K, Ostman A. High interstitial fluid pressure—an obstacle in cancer therapy. Nat Rev Cancer 2004;4:806–13.
32. Yang AD, Bauer TW, Camp ER, et al. Improving delivery of antineoplastic agents with anti-vascular endothelial growth factor therapy. Cancer 2005;103: 1561–70.
33. Weis SM, Cheresh DA. Pathophysiological consequences of VEGF-induced vascular permeability. Nature 2005;437:497–504.
34. Yuan F, Chen Y, Dellian M, et al. Time-dependent vascular regression and permeability changes in established human tumor xenografts induced by an anti-vascular endothelial growth factor/vascular permeability factor antibody. Proc Natl Acad Sci U S A 1996;93:14765–70.
35. Wildiers H, Guetens G, De Boeck G, et al. Effect of antivascular endothelial growth factor treatment on the intratumoral uptake of CPT-11. Br J Cancer 2003; 88:1979–86.
36. Huber PE, Bischof M, Jenne J, et al. Trimodal cancer treatment: beneficial effects of combined antiangiogenesis, radiation, and chemotherapy. Cancer Res 2005;65:3643–55.
37. Willett CG, Boucher Y, di Tomaso E, et al. Direct evidence that the VEGF-specific antibody bevacizumab has antivascular effects in human rectal cancer. Nat Med 2004;10:145–7.
38. Jain RK. Determinants of tumor blood flow: a review. Cancer Res 1988;48:2641–58.
39. Baish JW, Jain RK. Fractals and cancer. Cancer Res 2000;60:3683–8.
40. Segers J, Fazio VD, Ansiaux R, et al. Potentiation of cyclophosphamide chemotherapy using the antiangiogenic drug thalidomide: Importance of optimal scheduling to exploit the "normalization" window of the tumor vasculature. Cancer Lett 2006;244: 129–35.

Clinical Cancer Research

Bevacizumab-Induced Transient Remodeling of the Vasculature in Neuroblastoma Xenografts Results in Improved Delivery and Efficacy of Systemically Administered Chemotherapy

Paxton V. Dickson, John B. Hamner, Thomas L. Sims, et al.

Clin Cancer Res 2007;13:3942-3950.